Archives of Hydro-Engineering and Environmental Mechanics
Vol. 50 (2003), No. 2, pp. 85–106

Complete Solution for the Saturated Slopes in the Limit Stress State

Andrzej Batog, Elżbieta Stilger-Szydło

Wrocław University of Technology, Wybrzeże Wyspiańskiego 27, 50-370 Wrocław, Poland,
e-mail: szydlo@i14odt.iil.pwr.wroc.pl

(Received July 1, 2003; revised July 22, 2003)

Abstract

Complete solutions of saturated slopes in the limit state, in the aspects of statics and kinematics, are presented. The proposed methods can be applied to the calculation of stress fields and velocity fields and the estimation of the limit load for two basic (associated and non-associated with linear Mohr-Coulomb yield condition) flow rules. Samples of calculations for diverse saturation conditions appeared in slopes are included. The proposed methods will contribute to the extension of the use of limit state methods in engineering practice.

Key words: saturated slopes, limit stress state

1. Introduction

Earthworks, highway and water engineering projects provide an incentive for the creation of new technical conditions for earth structures, as regards: their basic parameters, fittings, the safety and environmental protection, and the assessment of the load capacity and stability of earth structures. Efforts are made to ensure the optimal design of slopes and embankments and the accurate prediction of their behaviour.

About a hundred methods of dimensioning slopes can be found in the literature. Very few attempts, however, have been made to evaluate the accuracy of such an impressive number of methods. The reason is the highly complex nature of the slope sliding phenomenon, which leads to the idealization of adopted physical models. Limit equilibrium and limit state stress methods predominate in the group of theoretical slope dimensioning methods.

The former methods presume that there is a limit state on some surfaces of a localized slip. A certain mechanism of deformation or failure along the slip surface is assumed and the force system associated with the mechanism is analyzed (Bishop 1955, Bishop and Morgenstern 1960, Morgenstern and Price 1965,

Spencer 1967, Izbicki and Mróz 1976, Chowdhury 1978, Sarma 1979, Janbu 1987). In the case of the so-called slice methods, there are proposals for estimating the stress on slip surfaces.

The limit state stress methods are based on a rigid, perfectly plastic model of the medium and assume that the limit state condition is fulfilled at each point of a considered area. The limit state theory in its static formulation enables the determination of the relationships between the shape of a slope, the limit load of the overburden and the state of stress in the whole mass (Sokolovsky 1960, Dembicki et al. 1964, Salençon (1972)). The kinematic method consists in seeking permissible deformation velocity fields corresponding to different mechanisms of flow (Drucker and Prager 1952, de Josselin de Jong 1959, Davis 1968, Drescher 1972, Chen 1975, Derski 1988, Drescher and Detournay 1993, Michalowski 1995).

The method mainly applied for seeking exact solutions is that of characteristics. For that method there are no solutions considering the field of the seepage forces. No comprehensive discussion of boundary problems of slopes in the limit state for different soil-water conditions can be found in the literature.

The aim of this paper is to present the complete solutions of slopes in the limit state, in the aspects of statics and kinematics for diverse soil-water conditions and boundary conditions appearing in slopes. The proposed methods will contribute to the extension of the use of limit state methods in engineering practice.

2. Statics in the Limit State

2.1. Homogeneous Soil Medium

The limit state theory distinguishes two basic types of problems in the case of slopes designing. The first type is a generalization of the bearing capacity problem where the shape of a slope is prescribed while the limit value of the load of its crest is to be determined. In the second type, the predetermined load on the crest is given and the stable slope shape is to be determined assuming that in the soil mass a limit equilibrium state occurs.

The problem of a slope profile determination is considered. An analysis of the quasi-static problem of the plane state of strain includes equations of equilibrium and the linear Mohr-Coulomb yield condition which represents the closest to experimental results hypothesis concerning the reaching of the state of equilibrium. Appropriate transformations lead to a system of two hyperbolic quasi-linear partial differential equations, written in a simple form (Sokolovsky 1960):

$$\frac{\partial \xi}{\partial x} + \tan(\zeta + \mu)\frac{\partial \xi}{\partial y} = a, \quad \frac{\partial \eta}{\partial x} + \tan(\zeta - \mu)\frac{\partial \eta}{\partial y} = b,$$
$$\left.\begin{matrix} a \\ b \end{matrix}\right\} = \mp \frac{\gamma_x \sin(\zeta \mp \mu) - \gamma_y \cos(\zeta \mp \mu)}{2\sigma \sin\phi \cos(\zeta \pm \mu)}. \tag{1}$$

The above equations are solved by the method of characteristics. The differential equations of characteristics and the relationships along them assume this form respectively:

$$\begin{aligned} \frac{dy}{dx} &= \tan(\zeta + \mu) \quad \frac{d\xi}{dx} = a; \quad \alpha \\ \frac{dy}{dx} &= \tan(\zeta - \mu) \quad \frac{d\eta}{dx} = b; \quad \beta \end{aligned} \tag{2}$$

where:

$$\mu = \frac{\pi}{4} - \frac{\phi}{2},$$

$$\sigma = 0.5(\sigma_x + \sigma_y) + c \cot\phi,$$

$$\xi = 0.5 \cot\phi \ln\frac{\sigma}{c} + \zeta,$$

$$\eta = 0.5 \cot\phi \ln\frac{\sigma}{c} - \zeta,$$

$$2\zeta = \xi - \eta,$$

ζ – the inclination of algebraically greater principal stress σ_1 to axis x,

ϕ – a soil internal friction angle,

γ_x, γ_y – the components of the dead weight,

α, β – the first and second family of characteristics, respectively, Fig. 1(a).

The stress components expressed by quantities σ, ζ are:

$$\sigma_x = \sigma(1 + \sin\phi\cos 2\zeta) - c\cot\phi, \qquad \sigma_y = \sigma(1 - \sin\phi\cos 2\zeta) - c\cot\phi,$$
$$\tau_{xy} = \sigma \sin\phi \sin 2\zeta. \tag{3}$$

The solution of the boundary problem of the slope profile determination consists in the simultaneous integration of Eqs. (2). This leads to the determination of the field of characteristics and the values of σ and ζ in net nodes for the prescribed static boundary conditions. The density of the net of characteristics increases.

The internal equilibrium condition and the boundary condition must be fulfilled also in the region situated outside the deformation field in the rigid zone, the plasticity condition must not be violated, but it has not to be satisfied, because the stress state below the plastic limit is admissible. The extended net of characteristics shown in Fig. 1b results from the solution of the initial-value problem along line AH and the characteristic problem, defined by known values, along lines AG and ACDB.

The determined stress field was confined, starting from point B, by stress discontinuity line BEFI. The stress field below this line was constructed in a

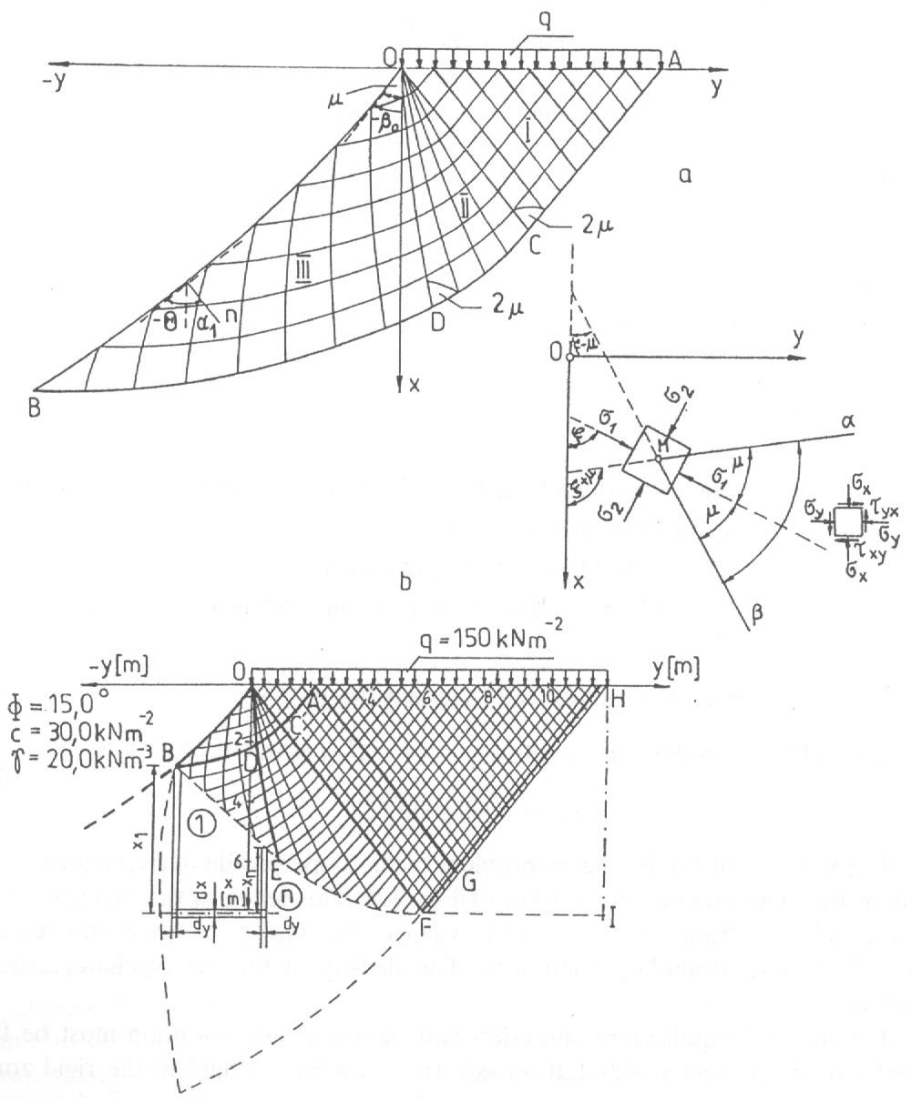

Fig. 1. Computational scheme for slope: (a) net of characteristics; (b) extension of stress field determined for slope plastic flow regions OBDCA on to adjacent rigid zones

way which ensured that the limit state was not exceeded at any place, no tensile stress occurred anywhere and the general directions of the stresses coincided with axes x, y. The direction of the discontinuity line at points where it intersects the characteristic of region BAGJ was determined taking into account the condition of constancy of stress σ_y at specified depth x.

The state of stress in vertical elements "1" and "n" with infinitely small width dy put up under point B, n is defined by these relations:

$$\sigma_{x(1)} = \sigma^*_{x(1)} + \gamma x_1, \quad \sigma_{y(1)} = \gamma x_1 \frac{1 - \sin\phi}{1 + \sin\phi}, \quad \sigma_{x(n)} = \sigma^*_{x(n)} + \gamma x_n, \tag{4}$$

where σ^* denotes the stress acting imnediately under the discontinuity line. The increase in vertical stress under the slope was assumed as lineal function of the depth.

For any point of the discontinuity line we can determine the parameters shown in Fig. 1b:

$$\sigma^*_{y(n)} = \bar{\eta}\left[\sigma^*_{x(1)} + \gamma\,(x_n - x_B)\right], \quad \bar{\eta} = \frac{1 - \sin\phi}{1 + \sin\phi} - \frac{2\overline{H}\sin\phi}{\sigma_{x(1)}\,(1 + \sin\phi)}, \tag{5}$$

where $\overline{H}$ is the tensile strength of the soil in the triaxial stress state, given by

$$\overline{H} = \frac{\sigma^*_{x(1)}\,(1 - \sin\phi)}{2\sin\phi}.$$

The state of stress below stress discontinuity line BEFI does not exceed limit state ($F(\sigma_{ij}) \leq 0$) of the medium.

2.2. Solution for Seepage through an Earthen Structures

The water conditions on the slopes and in the subsoil of the slope are a major factor determining the stability of such structures. Water filtering through the body of the slope changes the physical and mechanical properties of the soil, producing an extra load acting along stream lines on the soil skeleton. For steady non-pressure filtration, the equations of (flow) dynamics and the kinematic condition (liquid continuity equation) can be reduced to this homogeneous potential Laplace's equation:

$$\nabla^2 H = \nabla^2 p_w = 0, \tag{6}$$

where H is a hydraulic head function, p_w is water thrust.

Equation (6) can be solved in different ways. Numerical approximation is recommended for more complex shapes of filtration areas and boundary conditions.

Numerical approximation consists in replacing the potential changing continuously on the contour of a flat area with a system of values at the nodal points of a net plotted on this area. The solution to the first boundary problem for the Laplace equation is reached by replacing the derivatives with appropriate difference quotients. The obtained equation

$$p_{w_0} = \frac{p_{w_1} + p_{w_2} + p_{w_3} + p_{w_4}}{4} \tag{7}$$

used until convergence is achieved at all the nodal points constitutes a basis for the Liebmann iteration. Long and time-consuming iterative procedures, particularly near the filtration area contour, which does not coincide with the edge of the net area, can be handled only numerically.

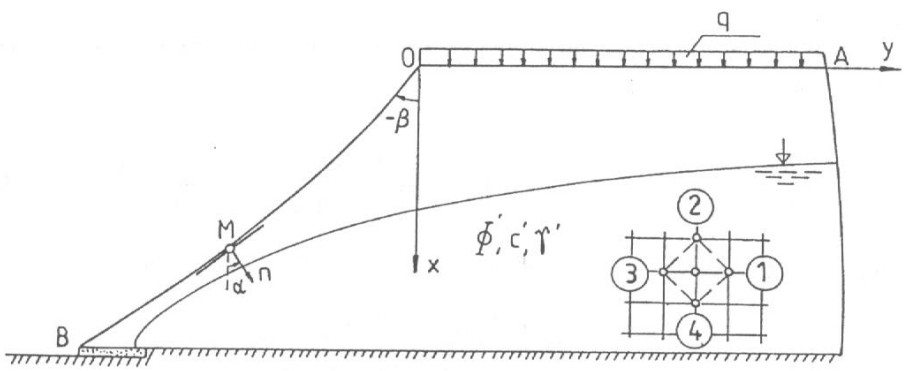

Fig. 2. Computational scheme for boundary condition of water saturated soil mass dewatered by horizontal flat draining system

The filtration forces included in the mass forces in Eqs. (1) enable us to solve the problem of the stability of a slope saturated with water (Fig. 2):

$$\begin{aligned}
&\frac{\partial \xi}{\partial x} + \tan(\zeta + \mu)\frac{\partial \xi}{\partial y} = \\
&\quad = \frac{-\left(\gamma_x' - \gamma_w \frac{\partial H}{\partial x}\right)\sin(\zeta - \mu) + \left(\gamma_y' - \gamma_w \frac{\partial H}{\partial y}\right)\cos(\zeta - \mu)}{2\sigma' \sin\phi' \cos(\zeta + \mu)}, \\
&\frac{\partial \eta}{\partial x} + \tan(\zeta - \mu)\frac{\partial \eta}{\partial y} = \\
&\quad = \frac{\left(\gamma_x' - \gamma_w \frac{\partial H}{\partial x}\right)\sin(\zeta + \mu) - \left(\gamma_y' - \gamma_w \frac{\partial H}{\partial y}\right)\cos(\zeta + \mu)}{2\sigma' \sin\phi' \cos(\zeta - \mu)},
\end{aligned} \tag{8}$$

where:

$\gamma_w \frac{\partial H}{\partial x}$, $\gamma_w \frac{\partial H}{\partial y}$ – components of seepage forces,

γ'_x, γ'_y – the components of the dead weight with water thrust included,

γ_w – the unit weight of water.

If the hydraulic gradient head is zero, then Eqs. (8) are reduced to (1).

3. Kinematics of the Limit State

The kinematics determines the state of the velocity of particles of the medium described by a rigid-plastic model. It assumes a physical relationship linking stress tensor σ_{ij} to strain rate tensor $\dot{\varepsilon}_{ij}$:

$$\dot{\varepsilon}_{ij} = \lambda \frac{\partial G(\sigma_{ij})}{\partial \sigma_{ij}} = -\frac{1}{2}\left(\frac{\partial v_i}{\partial x_j} + \frac{\partial v_j}{\partial x_i}\right), \tag{9}$$

where λ is a non-negative (can be zero), v_i are velocity vector components and $G(\sigma_{ij})$ is the following plastic potential

$$G(\sigma_{ij}) = \sigma_1 - \sigma_2 + (\sigma_1 - \sigma_2)\sin\psi - 2c\cos\psi = 0 \quad 0 \le \psi \le \phi. \tag{10}$$

For $\psi = \phi$ we have $G(\sigma_{ij}) = F(\sigma_{ij})$ and Eq. (10) represents the associated flow rule, for $\psi < \phi$ Eq. (10) represents the non-associated flow rule, ψ is a dilatation angle which determines change in the volume of the medium. If the isotropy condition and relations (9) and (10) are used, differential equations of velocity characteristics and relationships occurring along them are obtained (Jenike and Shield 1959):

$$\begin{aligned} &\frac{dy}{dx} = \tan(\zeta + \mu^*) \quad dv_{\alpha'} - (v_{\alpha'}\tan\psi - v_{\beta'}\sec\psi)d\zeta = 0; \quad \alpha', \\ &\frac{dy}{dx} = \tan(\zeta - \mu^*) \quad dv_{\beta'} + (v_{\beta'}\tan\psi - v_{\alpha'}\sec\psi)d\zeta = 0; \quad \beta', \end{aligned} \tag{11}$$

where $v_{\alpha'}, v_{\beta'}$ are projections of the velocity vector on to appropriate directions of characteristics α' and β', $\mu^* = \frac{\pi}{4} - \frac{\psi}{2}$.

The linearity of Eqs. (11) is the reason why the field of velocity characteristics does not depend on the kinematic boundary conditions, but only on the form of the field of stress characteristics. A boundary condition assuming a rigid block with known velocity $v(y)$ of its points at the top of the slope is proposed. This may correspond to loading with a rigid foundation.

The problem is analysed for the general case where the non-associated flow rule is applied. The assumed kinematic boundary conditions were analysed for the problem of slope profiling. The lineal growing load on the slope crest is placed on the rigid block, Fig. 3. In particular case for $\delta_1 = 0$ the load is uniform. The

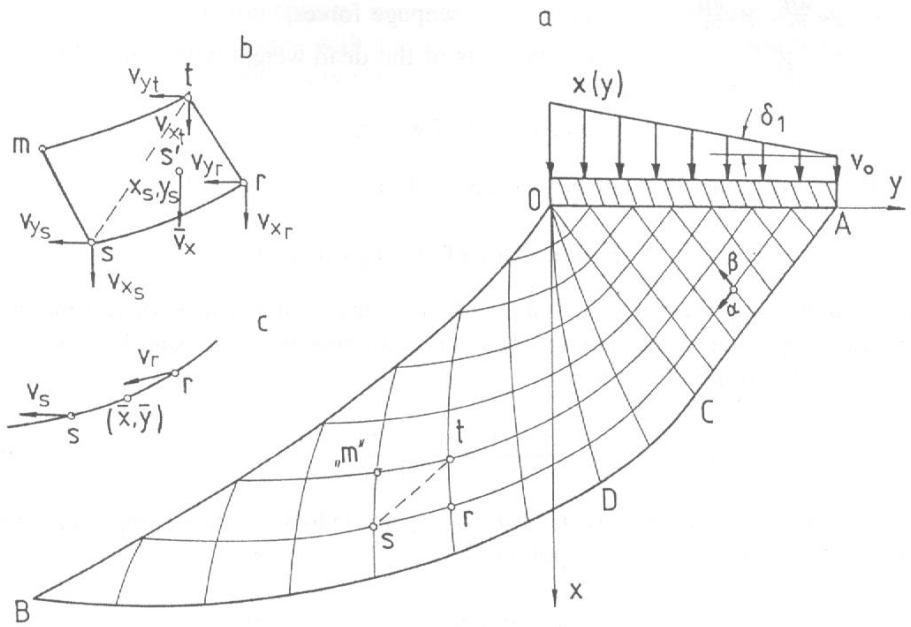

Fig. 3. Determination of velocity field and dissipation power for associated flow rule: (a) general scheme; (b), (c) subsidiary sketches

starting point for this analysis is a net of characteristics obtained from the static solution. That net determines the range of the motion zone in the soil mass. The boundary between the motion zone and the soil at rest is determined by the velocity characteristic drawn from point A to B on the slope profile. The characteristic AB is also the discontinuity line.

The rigid block is moving with velocity v_o along OA under the influence of the load. Component $v_x(y)$ of the velocity of this block is given by this relation:

$$v_x(y) = v_o + \frac{(y_A - y)v_o\gamma \tan\delta_1}{c}. \tag{12}$$

Boundary conditions (12) along OA may be regarded as kinematically permissible since:

$$|\dot{\varepsilon}_1| \leq |\dot{\varepsilon}_2| \quad \dot{\varepsilon}_1 = (1 - \sin\psi)\frac{\tan\delta_1}{\cos\psi}, \quad \dot{\varepsilon}_2 = -\frac{(\sin\psi + 1)\tan\delta_1}{\cos\psi}, \tag{13}$$

$$\dot{\varepsilon} = \dot{\varepsilon}_1 + \dot{\varepsilon}_2 = -2\tan\delta_1 \tan\psi, \quad \lambda = \frac{\tan\delta_1}{\cos\psi}. \tag{14}$$

A correct kinematic solution should provide for the flow of the material, satisfy the boundary conditions, and assure non-negative increment of work dissipated

at every point in the whole area of plastic flow. Because of the assumed absence of friction at the block-medium contact, the power dissipated along OA is equal to zero for any velocity of block $v(y)$.

Along section AC' of the discontinuity line and within the volume of area OAC', the dissipated power is equal to:

$$D_L^{AC'} = \frac{1}{\sin\mu^* \cos\mu^*} \times$$
$$\times \left\{ \left[\cos\phi + \frac{\sin\phi - \sin\psi}{1+\sin\phi}(q - \cos\phi) \right] x_{C'} + x_{C'}^2 \frac{\sin\phi - \sin\psi}{2(1+\sin\phi)} \right\} > 0, \tag{15}$$

$$D_V^{OAC'} =$$
$$= 4x_{C'} \tan\delta_1 \sec\psi \left[\cos\phi \left(y_C - \frac{1}{2} x_{C'} \tan\mu^* \right) \left(1 - \frac{\sin\phi - \sin\psi}{1+\sin\phi} \right) + \right. \tag{16}$$
$$\left. + \frac{1}{q} \left(\frac{q}{2} x_{C'} y_C + y_C - \frac{\tan\mu^*}{2} - x_{C'} - \frac{1}{3} q x_{C'}^2 \tan\mu^* \right) \frac{\sin\phi - \sin\psi}{1+\sin\phi} \right] \geq 0.$$

For the associated flow rule (when $\psi = \phi$) Eqs. (15) and (16) are reduced to (17):

$$D_L^{AC} = \frac{\cos\phi}{\sin\mu \cos\mu} x_C > 0,$$
$$D_V^{OAC} = 4x_C \tan\delta_1 \left(y_C - \frac{1}{2} x_C \tan\mu \right) \geq 0. \tag{17}$$

A computational scheme for the determination of the velocity field and the dissipation power in area OCDB of the slope (for both flow rules) is shown in Figs. 3 and 4.

The net of characteristics determined for the stress field is at the same time a net of velocity characteristics for the associated flow rule. Taking into account the velocity characteristics and the kinematic boundary conditions along OA determined according to Eq. (12), the mixed problem for area OAC and the characteristic problem for area OCDB are solved.

The system of Eqs. (11), written in a differential form, is put to use in the numerical determination of the velocity field at the nodal points of area OCDB. Then the solution along OC and relationships along discontinuity line CDB in this form:

$$v_\alpha = \frac{\cos\phi}{\sin\mu} \exp\left[\left(\zeta - \frac{\pi}{2} \right) \tan\phi \right] \quad v_\beta = 0 \tag{18}$$

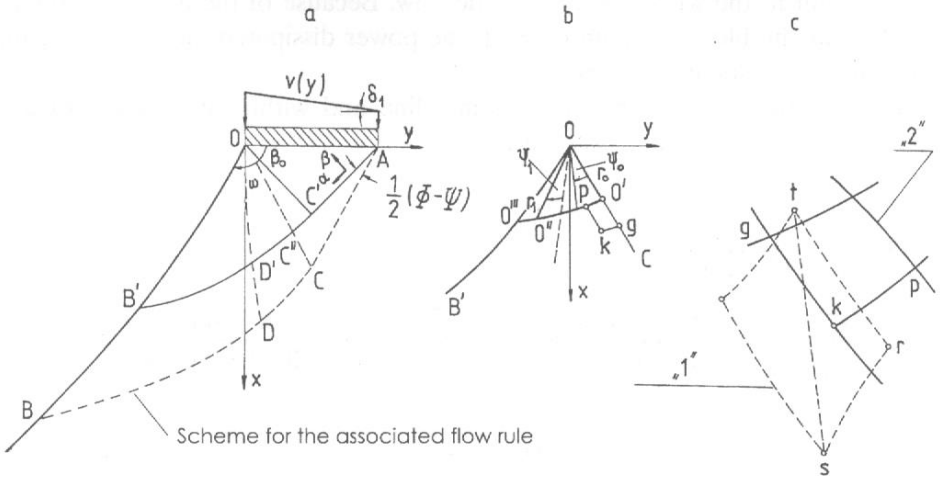

Fig. 4. Determination of velocity field for non-associated flow rule: (a) general scheme; (b), (c) subsidiary sketches ("1" net of stress characteristics, "2" net of velocity characteristics)

are used. The computing accuracy is improved by applying the mean function method.

For the non-associated flow rule, the net of velocity characteristics does not coincide with that of stress characteristics. It does not depend on the kinematic boundary conditions but only on the form of the field of stress characteristics.

Within area OAC′ (Fig. 4), the net of velocity characteristics consists of two families of parallel straight lines deviating from the stress characteristics by an angle equal to $0.5(\phi - \psi)$. The net does not contain a fan.

A velocity field for the non-associated flow rule is determined in a similar way as for the rule presented above associated with the condition of plasticity. The velocity discontinuity line here is characteristic α' (AC′C″D′B′) and the velocities along it are as follows:

$$v_{\alpha'} = \frac{\cos\psi}{\sin\mu^*} \exp\left[\left(\zeta - \frac{\pi}{2}\right)\tan\psi\right] \quad v_{\beta'} = 0. \tag{19}$$

After determining the velocity components (v_α and v_β or $v_{\alpha'}$ and $v_{\beta'}$) at each node of the net of characteristics (for area OC′C″D′B′or OCDB), numerical calculations of the dissipation power for the two flow rules, respectively, are performed. A method similar to the finite element method is recommended for this purpose.

The dissipation power values in areas OAC and OAC′ are given by Eqs. (15)÷(17). The dissipation power in the remaining area is approximated by an unknown velocity function for area OCDB (OC′C″D′B′) using a series of values $v(x, y)$ calculated at the particular nodal points of the net of characteristics.

For a current point of an area divided into triangular elements with vertices r, s, t, we can write:

$$v(x,y) = \begin{Bmatrix} v_x(x,y) \\ v_y(x,y) \end{Bmatrix} = [N_r, N_s, N_t] \begin{Bmatrix} v_r \\ v_s \\ v_t \end{Bmatrix}, \tag{20}$$

where the assumed linear shape functions, given generally for the m-th element, are defined by the following relations:

$$N_\gamma = \frac{a_\gamma x + b_\gamma y + c_\gamma}{2\Delta}, \quad \gamma = r, s, t \tag{21}$$

(2Δ is a double area of triangle r, s, t and coefficients $a_r, ..., c_t$ are obtained through the cyclical transposition of the indices).

We can determine the dissipation power in a finite number of elements of area OCDB or OC′C″D′B′ by using the following relations:

$$D_V^{OCDB} = \cos\phi \sum_{i=1}^{n} \sqrt{\left(\dot{\varepsilon}_{x_i} - \dot{\varepsilon}_{y_i}\right)^2 + 4\left(\dot{\varepsilon}_{(xy)_i}\right)^2}\,\Delta_i h \tag{22}$$

for the associated flow rule or

$$D_V^{OC'C''D'B'} = \\ = \sum_{i=1}^{n} \sqrt{\left(\dot{\varepsilon}_{x_i} - \dot{\varepsilon}_{y_i}\right)^2 + 4\left(\dot{\varepsilon}_{(xy)_i}\right)^2}\,[\cos\phi + (\sigma_i - \cot\phi)(\sin\phi - \sin\psi)]\Delta_i h \tag{23}$$

for the non-associated flow rule, where h is the element's thickness equal to unity, σ_i is the stress in centroid $S(x_o, y_o)$ of triangular element r, s, t.

The dissipation power values along discontinuity lines CDB and C′C″D′B′ are calculated by applying the following formulas:

$$D_L^{CDB} = \cos\phi \sum_{k=1}^{m} v_{\alpha k}\,\Delta l_k \cdot 1, 0, \\ D_L^{C'C''D'B'} = \sec\psi \sum_{k=1}^{m} v_{\alpha_k'}\,[\cos\phi + (\overline{\sigma}_k - \cot\phi)(\sin\phi - \sin\psi)]\,\Delta l_k \cdot 1, 0, \tag{24}$$

where $\overline{\sigma}_k$ is the stress in centroid $S(x_o, y_o)$ of triangular element r, s, t and Δl_k is the area of this nodal triangular element.

The total dissipation power is the sum of the volumetric dissipation of OACDB or OAC′C″B′ and the dissipation along discontinuity line ACDB or AC′C″D′B′ for the two flow rules, respectively. Whereas power of the force of gravity is expressed by this relation:

$$L = \sum_{i=1}^{n} v_{x_i}(x_s, y_s)\,\Delta_i \cdot 1,0, \tag{25}$$

where $v_{x_i}(x_s, y_s)$ is determined from formula (20).

The upper estimate of limit load q_k when the flow rule associated with the condition of plasticity is applied and the estimate of load q_{k_1} for the non-associated flow rule can be determined on the basis of limit load capacity theorems (Chen 1975, Drescher and Detournay 1993). If the power balance equation is used and $q_k(y) = \text{const.}$ and $q_{k_1}(y) = \text{const.}$ are assumed, the following is obtained:

$$\left.\begin{matrix} q_k \\ q_{k_1} \end{matrix}\right\} = \frac{2(D-L)}{y_A(2 + y_A \tan\delta_1)}, \tag{26}$$

where D is the total internal dissipation, the sum of the volumetric dissipation of OACDB and the dissipation along discontinuity line ACDB.

Dependence of kinematic estimates of load q_{k_1} on the dilatation angle ψ was shown in Fig. 5, where $\bar{n} \geq 2$ is a numerical multiplier and q_s is the static load.

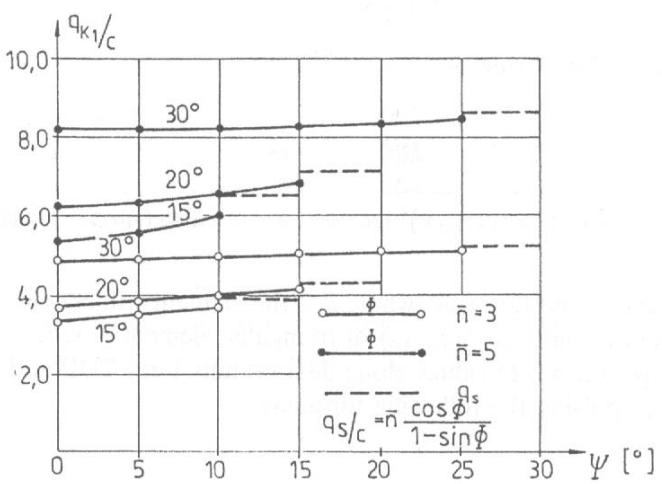

Fig. 5. Dependence of kinematic estimates of load q_{k_1} on the dilatation angle ψ

4. Results of Numerical Calculations and Samples

The prediction of optimum shapes of slopes (newly raised or made in virgin soil), the forecasting of their behaviour and the assessment of the stability of the slopes are major problems in civil construction and mining. Solutions to them should be sought on the basis of the mathematically exact theory of limit states from which relationships between the shape of the slope, the limit loading of the overburden

and the state of stress in the soil mass follow (Dembicki 1967, Salençon 1972). The final solution will be affected by the diversity of soil-water conditions, the values of geotechnical parameters and the geometry and loading of the earth structure.

4.1. Dry Slopes

The solution of the boundary problem of the slope profile determination consists in the simultaneous integration of Eqs. (2). This leads to the determination of the field of characteristics and the coordinates of the nodes prescribes the slope final shape. Figs. 6, 7, 8 show the influence of a change in the basic geotechnical parameters of the soil (soil bulk density γ, cohesion c, angle of internal friction ϕ) and in the overburden load on the shape of the profile of a slope with limited stability.

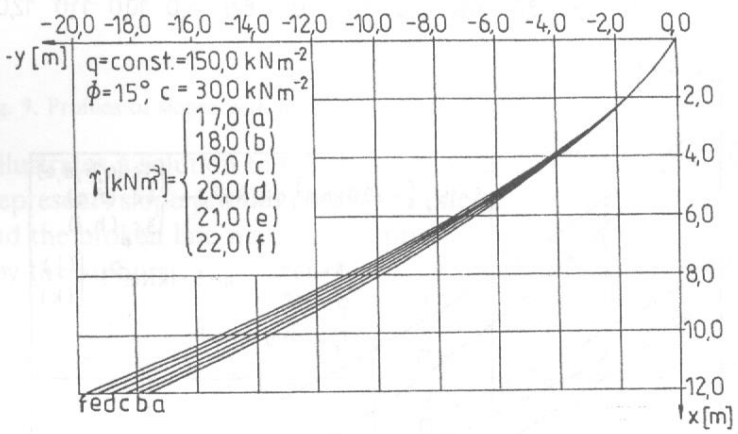

Fig. 6. Influence of γ on shape of slope's profile $[q > q_{\min} = 2c\cos\phi/(1-\sin\phi)]$

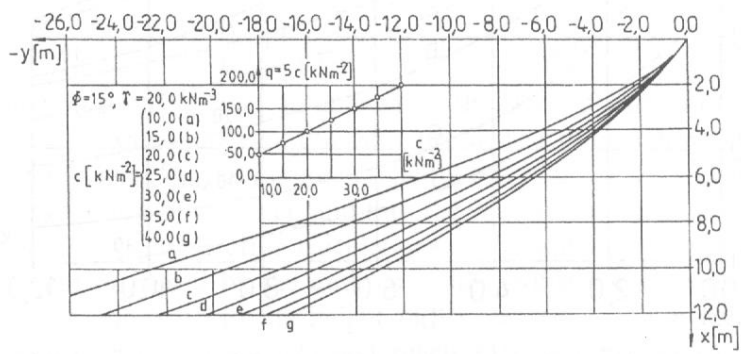

Fig. 7. Influence of soil cohesion c on shape of slope's profile $(q > q_{\min})$

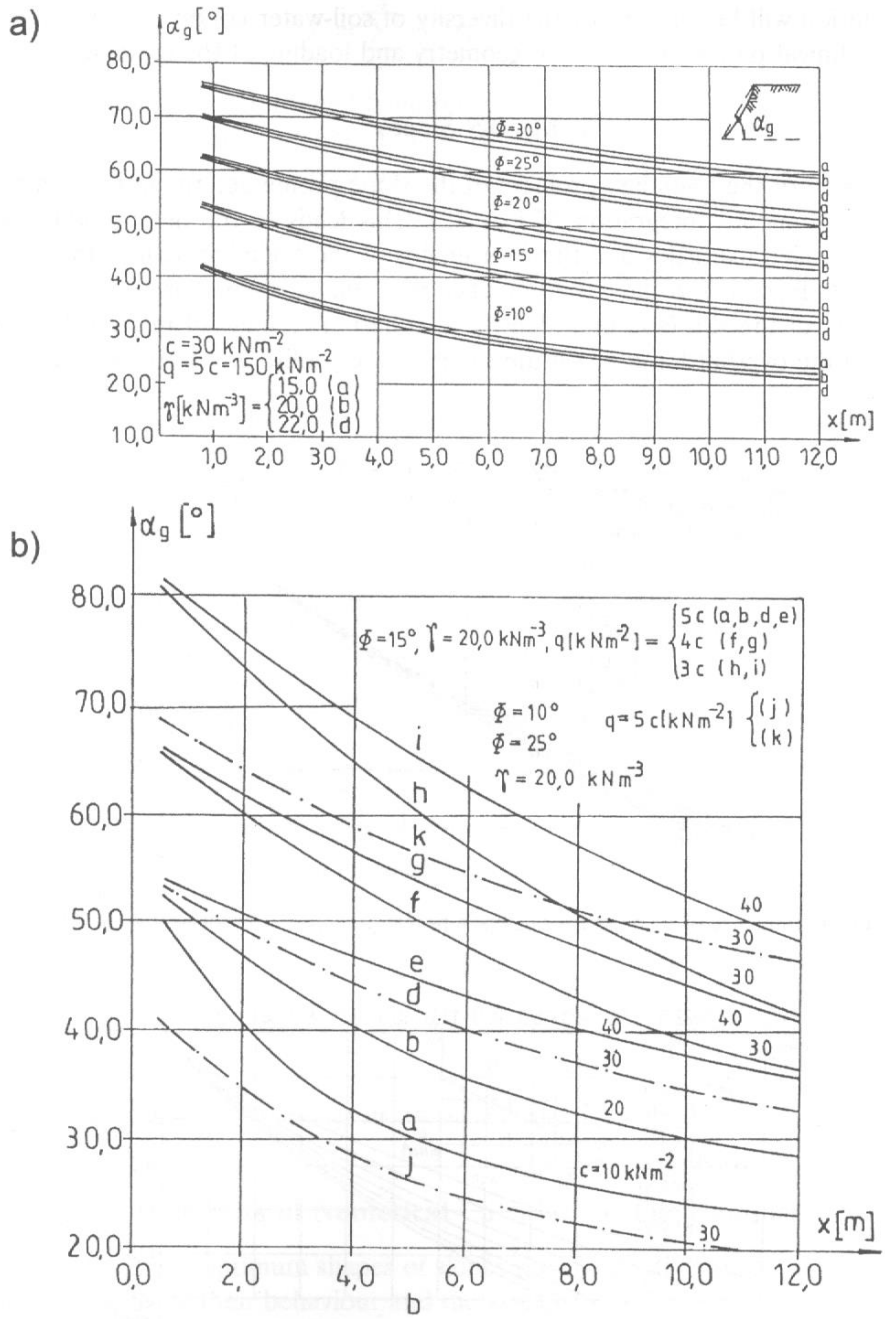

Fig. 8. Relationship between general angle of slope α_g and its height: (a) for different values ϕ and γ; (b) for different overburden load values q

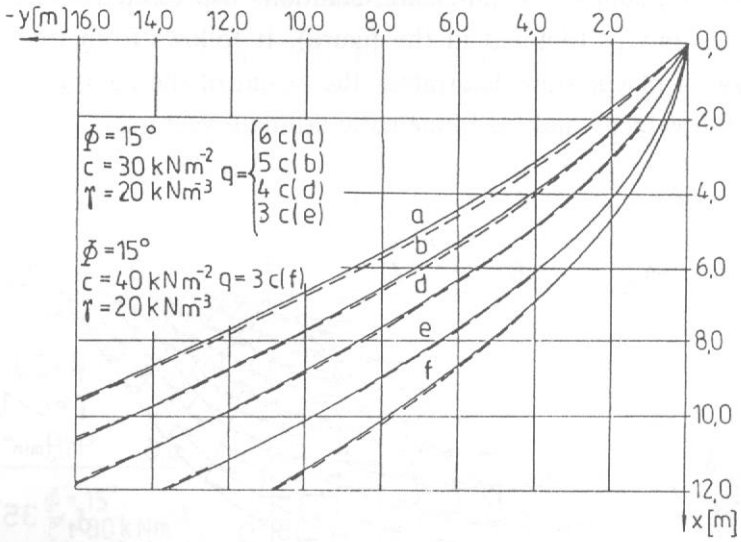

Fig. 9. Profiles of slopes with limited stability [—— Eqs. (1), - - - - Eq. (27)]

Fig. 9 illustrates a solution to the statics of a homogeneous infinite slope. The solid line represents slope profiles obtained from the numerical solution of system Eqs. (1) and the broken line marks slope profiles calculated by applying Eq. (27) proposed by the authors:

$$
\begin{aligned}
y &= -\frac{2c(1+\sin\phi)}{\gamma(1-\sin\phi)}\left(\frac{1}{2}\theta^2 - \frac{2}{3}\theta^3\tan\phi + \frac{1+6\tan^2\phi}{12}\theta^4 + \right. \\
&\quad \left. -\frac{1}{2}\beta_o^2 + \frac{2}{3}\beta_o^3\tan\phi - \frac{1+6\tan^2\phi}{12}\beta_o^4\right), \\
\theta &= -\frac{1}{2\tan\phi}\ln\left[\frac{(\gamma x + q + c\cot\phi)(1-\sin\phi)}{c\cot\phi(1+\sin\phi)}\right] \\
\beta_o &= \frac{\cot\phi}{2}\ln\left[\left(\frac{q}{c\cot\phi}+1\right)\frac{1-\sin\phi}{1+\sin\phi}\right] < 0.
\end{aligned}
\tag{27}
$$

Equation (27) resulted from an analysis of the state of stress in three plastic areas of the slope. An equation of the slope profile was obtained, which was then rearranged by replacing it with a finite number of terms of a series expansion. Four terms of the expansion of the integrand into the Maclaurine series are enough to apply formula (27) to engineering calculations of the stability of slopes.

The equation proposed by the authors yields profile curves coincident with the numerical solutions up to the height of 10 c/γ (in medium cohesive soils and firm cohesive ground this height may reach 20.0÷30.0 m). Above this height the accuracy of the obtained results decreases as the slope's height and load q increase, but it increases with increasing ϕ and c.

Fig. 10 shows examples of kinematic solutions expressed by dimensionless quantities x', y' and v_o (defined in the figure). It follows from them that the choice of a law of plastic flow determines the extent of the zone of motion and the values of the velocity and load kinematic estimate vectors.

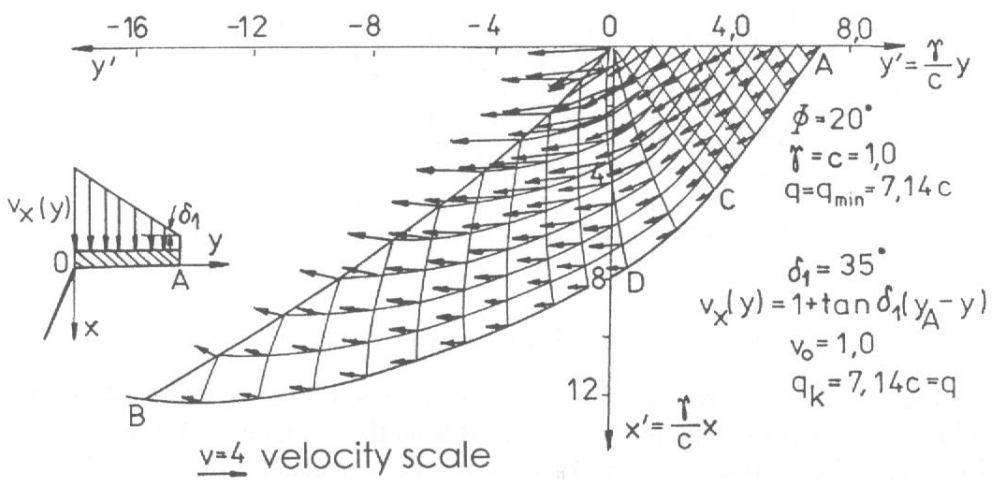

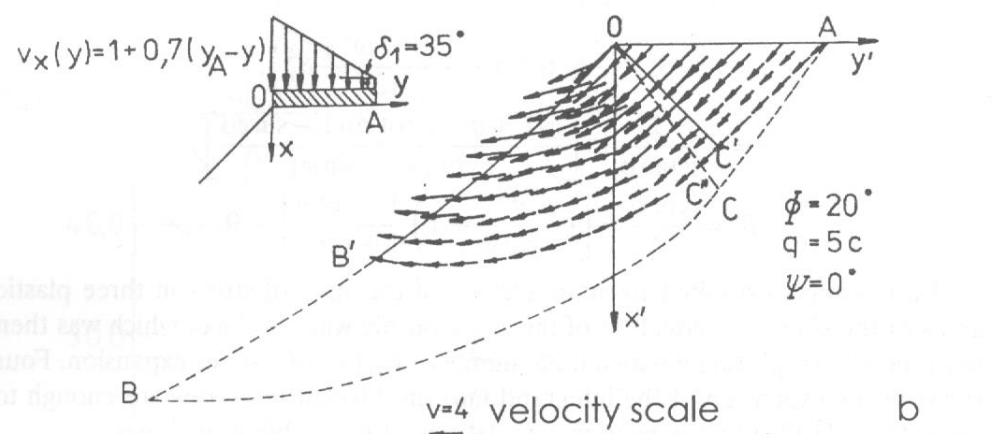

Fig. 10. Kinematic solution: (a) velocity field in the case of the associated flow rule; (b) velocity field in the case of the non-associated flow rule

4.2. Saturated Slopes

Three cases were considered: water filtering through the soil mass of the slopes, fully saturated slopes and slopes sprinkled by rainfall. The examples of solutions obtained for analyzed cases in Figs. 11–13 are presented. The slope angle of the profile of saturated soil mass in the limit state depends on: the values of the body's and the subsoil's geotechnical parameters, the filtration area geometry and the overburden load. The comparison of the profiles of slopes calculated for the diverse water condition is presented in Fig. 14. Saturated slopes are much gentler than the ones without filtration.

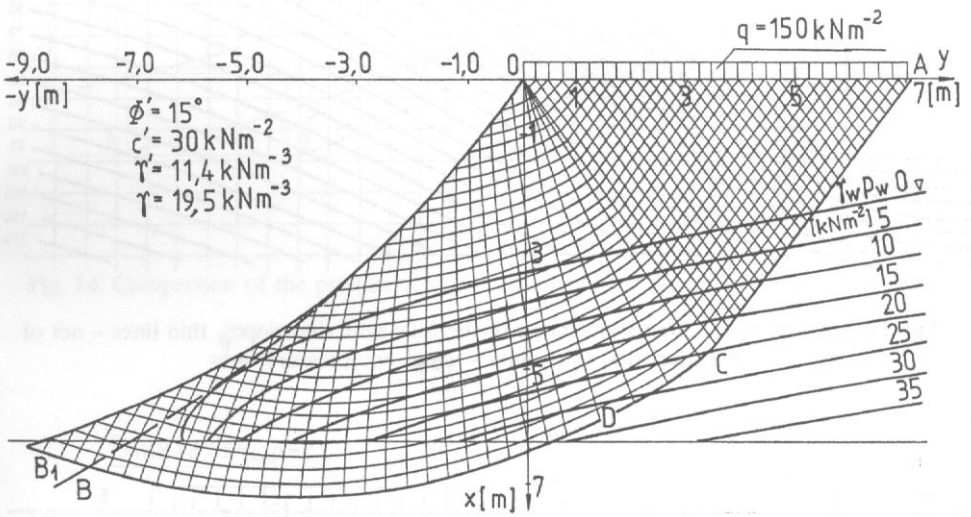

Fig. 11. Solution of the limit state statics of the slope located on the impermeable subsoil with the groundwater filtering through the soil mass

Complete presentation of all considered cases is not possible. Comprehensible analyses of the limit state for different water patterns in the soil mass and ground permeabilities can be found in papers by Stilger-Szydło and Kisiel (1980) and Skoczylas and Stilger-Szydło (1986).

4.3. Results Assessment

Due to limited available literature on the limit state analysis for slopes with the water flow, verification of the present work is possible by comparison with the published solutions of the slope dimensioning problem for dry soil masses. For that comparison we calculate the bearing capacity factors N_c and N_γ respectively defined in foundation engineering by:

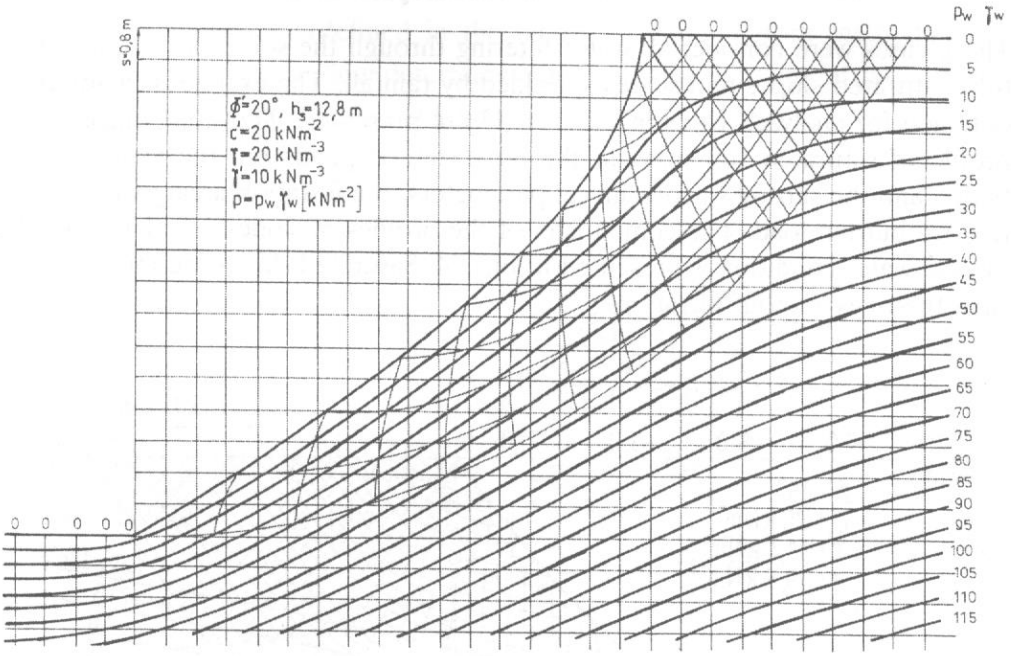

Fig. 12. Solution of the limit state statics of the fully saturated slopes, thin lines – net of characteristics, thick lines – water equipressure lines

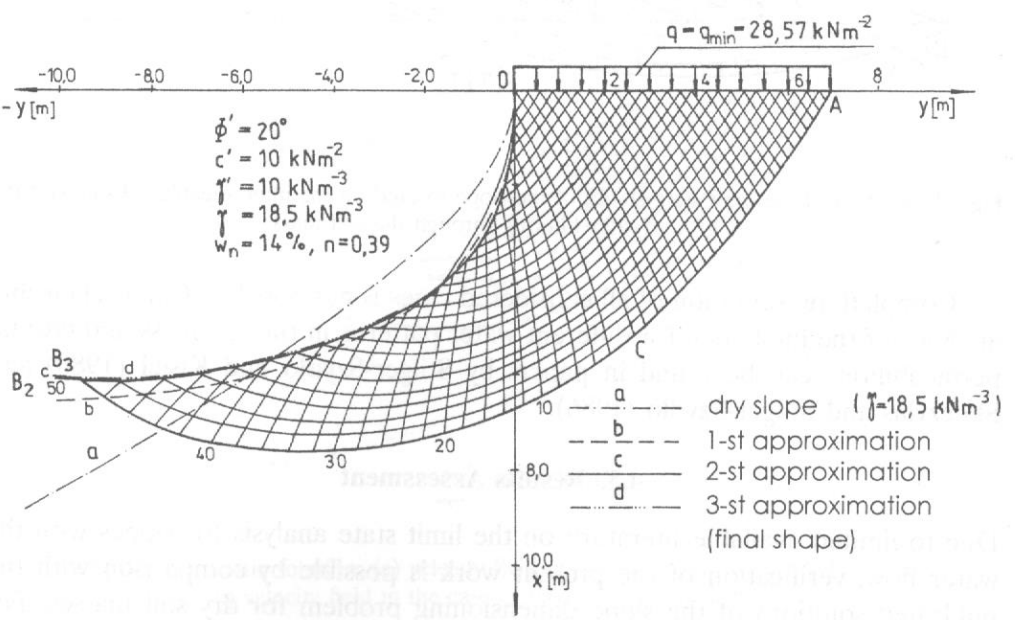

Fig. 13. Solution of the limit state statics of the slope, sprinkled by the rainfall

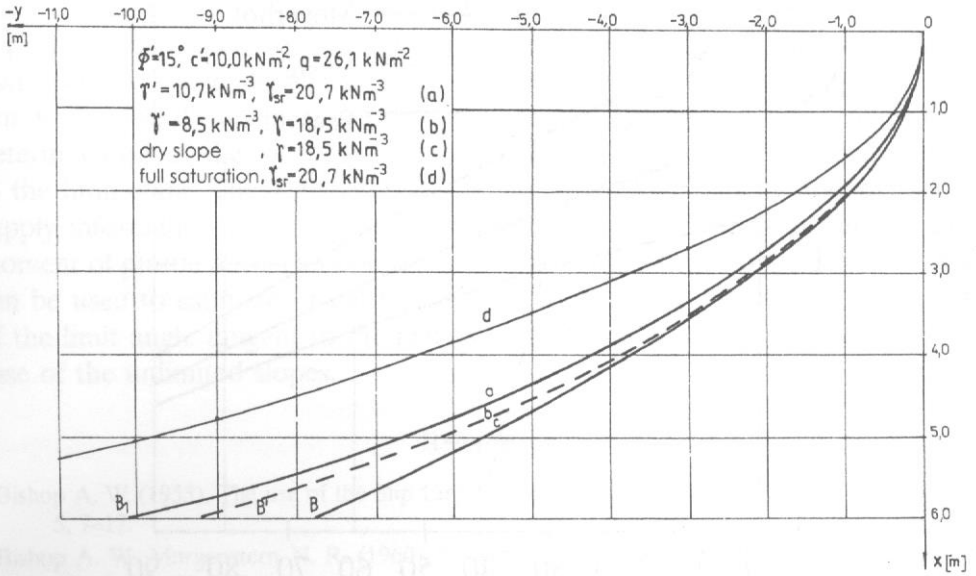

Fig. 14. Comparison of the profiles of slopes calculated for the diverse water condition

$$N_c = \left[N_\gamma - 1\right] \cot \phi,$$
$$N_\gamma = e^{\pi \tan \phi} \tan\left(\frac{\pi}{4} + \frac{\phi}{2}\right) \tag{28}$$

using the method of characteristics for homogeneous soil medium Eqs. (1), (2). The N_c values, indicate the share of the weightless soil in the entire bearing capacity, obtained here agree well with those by Meyerhof (1951), while Vesic's (1975) reduction relation becomes very conservative as the slope gets steeper (Fig. 15).

The present N_γ values, indicating the influence of dead weight of soil in the entire bearing capacity, are lower than others, given by Mizuno et al. (1960), Graham et al. (1988). The comparison of N_γ values are shown in Fig. 16. These results are obtained from static solution and the are the lower bound. The present solution is on the safe side.

5. Conclusions

This work presented solutions for analysis of the saturated slopes in the limit state. This is the essential contribution to the development of the theory of limit load-carrying capacity. A wide range of boundary conditions was considered by varying the soil parameters and water-soil conditions.

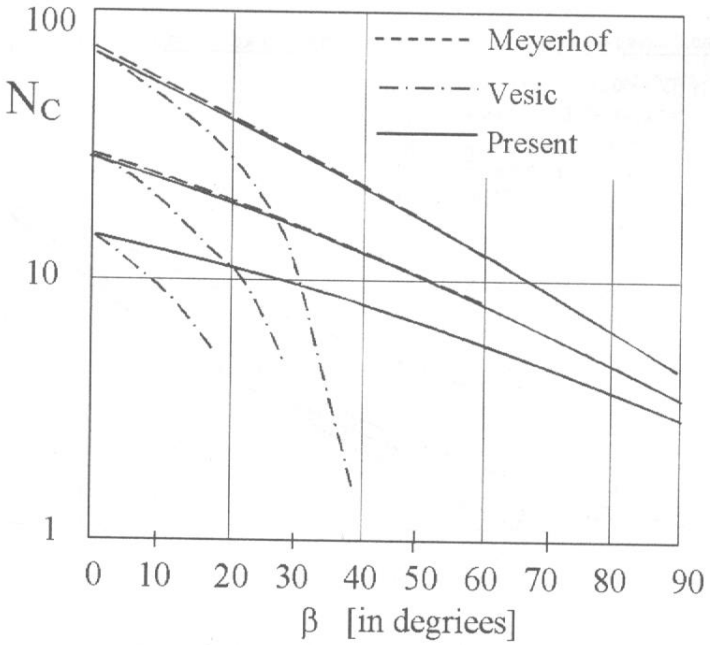

Fig. 15. Comparison of N_c values with those of Meyerhof (1951) and Vesic (1975) for different friction angle (after Sarma and Chen 1995)

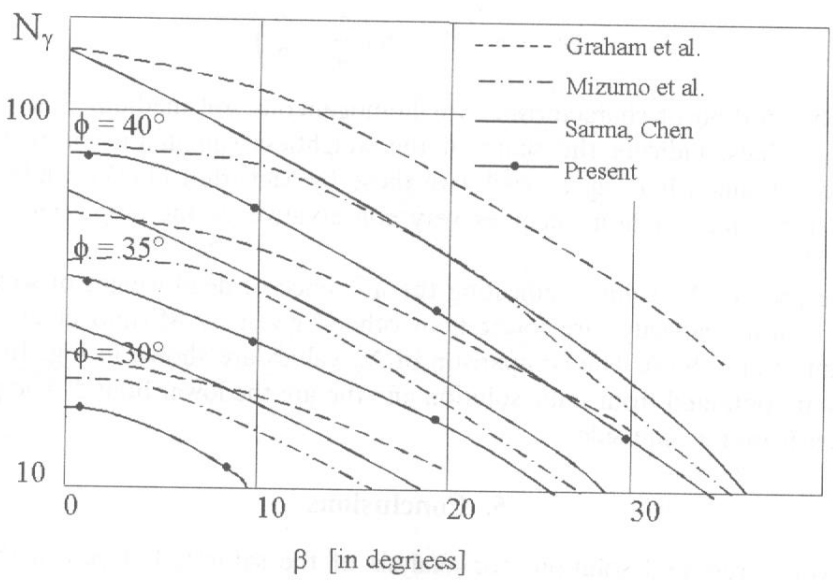

Fig. 16. Comparison of N_γ values with those of Mizumo et al. (1960), Graham et al. (1988) and Sarma, Chen (1995) (after Sarma and Chen 1995)

The basic problem of a slope profile determination was considered. Presented static and kinematic solutions, solved using the method of characteristics, can be applied to the calculation of stress fields and velocity fields for associated and non-associated with the linear Mohr-Coulomb yield condition flow rules. They can be successfully applied for practical purposes. The static solution leads to the determination of the field of characteristics and prescribes the shape of slopes in the limit state. The kinematic solution based on the velocity hodographs can supply information as to the slope behaviour and its deformations at the initial moment of plastic flow. The averaging, general angle of the slope in the limit state can be used to estimate of the factor of safety value (FOS) defined as the ratio of the limit angle tangent to the real slope angle tangent, in a similar way to the case of the unlimited slopes.

References

Bishop A. W. (1955), The use of the Slip Circle in the Stability Analysis of Slopes, *Geotechnique*, 5, 7–17.

Bishop A. W., Morgenstern N. R. (1960), Stability Coefficients for Earth Slopes, *Geotechnique*, 10, No. 4, 129–150.

Chen W. F. (1975), *Limit Analysis and Soil Plasticity*, Elsevier, Amsterdam.

Chowdhury R. N. (1978), *Slope Analysis*, Elsevier, Amsterdam.

Davis E. H. (1968), *Theories of Plasticity and the Failure of Soil Masses*, [In:] *Soil Mechanics: Selected Topics* , (ed. I. K. Lee), 341–380, London, Butterworth.

Dembicki E., Kravtchenko J., Sibille R. (1964), Sur les Solutions Analitiques Approchées de Problémes d'Équilibre Limite Plan pour Milieux Cohérents et Pésants, *Journal de Mécanique*, Paris, No. 3.

Dembicki E. (1967), Profils des Talus des Massifs en Équilibre Limite à Surface Plane Horizontale Surchrgeé, *Bull. Acad. Polon. Sci., Ser. Sci. Tech.*, 15, 4.

Derski W., Izbicki R. J., Kisiel I., Mróz Z. (1988), *Rock and Soil Mechanics*, Elsevier, Amsterdam.

Drescher A. (1972), Some Remarks on Plane Flow of Granular Media, *Arch. Mechaniki Stosowanej*, 24, 837–848.

Drescher A., Detournay E. (1993), Limit Load in Translational Failure Mechanisms for Associative and Non-associative Materials, *Geotechnique*, 43, No. 3, 443–456.

Drucker D. C., Prager W. (1952), Soil Mechanics and Plastic Analysis or Limit Design, *Q. Appl. Math.*, 10, No. 2, 157–165.

Graham J., Andrews M., Shields D. H. (1988), Stress Characteristics for Shallow Footings in Cohesionless Slopes, *Can. Geotech. J.*, 25(2), 238–249.

Izbicki R. J., Mróz Z. (1976), *Limit Analysis Methods in Soil and Rock Mechanics* (in Polish), PWN, Warszawa.

Janbu N. (1987), *Slope Stability Computations*, [In:] *Embankment–dam Engineering, Casagrande Volume*, ed. R. C. Hirschfeld and S. J. Poulos, Krieger Pub. Co., 47–86.

Jenike A. W., Shield R. T. (1959), On the Plastic Flow of Coulomb Solids Beyond Original Failure, *Journ. Appl. Mech., Trans. ASMF*, 27, 599–607.

Josselin de Jong G. de (1959), *Statics and Kinematics in the Failable Zone of a Granular Material*, Delft, Waltman.

Meyerhof G. G. (1951), The Ultimate Bearing Capacity of Foundations on Slopes, *Geotechnique*, 2 (4), 301–332.

Michalowski R. L. (1995), Slope Stability Analysis: a Kinematical Approach, *Geotechnique*, 45, No. 2, 283–239.

Mizuno T., Tokumitsu Y., Kawakami H. (1960), On the Bearing Capacity of a Slope of Cohesionless Soil, *Soil and Foundations*, 1(2), 30–37.

Morgenstern N. R., Price V. E. (1965), The Analysis of the Stability of General Slip Surfaces, *Geotechnique*, 15, No. 1, 79–93.

Salençon J. (1972), Butée d'une Paroi Lises sur un Massif Plastique, Solutions Statiques, *Journal de Mécanique*, Paris, No. 11, 1, 135–146.

Sarma S. K. (1979), Stability Analysis of Embankments and Slopes, *Journal Geotech. Engineering Div., ASCE*, 105, No. 12, 1511–1524.

Sarma S. K., Chen Y. C. (1995), Seismic Bearing Capacity of Shallow Strip Footings near Sloping Ground, *European Seismic Design Practice*, Ed. Elnashai, Balkema, 505–512.

Skoczylas K., Stilger-Szydło E. (1986), Analysis of Stability of Embankments, Seepage Forces being taken into Account, *Studia Geotechnica et Mechanica*, 8, No. 4, 3–15.

Sokolovsky V. V. (1960), *Statics of Soil Media*, 2nd ed., Butterworths, London.

Spencer E. (1967), A Method of Analysis of the Stability of Embankments Assuming Parallel Inter–slice Forces, *Geotechnique*, 17, No. 1, 11–26.

Stilger-Szydło E., Kisiel I. (1980), *Le champ des Forces de Filtration dans l'etendue d'un Talus en Etat Limite de la Stabilite*, PWN, Serie De Mec. Appl., Varsovie, 551–560.

Vesic A. S. (1975), Bearing Capacity of Shallow Foundations, Foundation Engineering Handbook, 1st edn., H. F. Winterkorn, H. Y. Fang (eds.), Chap. 3, Van Nostrand Reinhold Co. Inc., New York, 121–147.